J. Z. Sun

Spin angular momentum transfer in current-perpendicular nanomagnetic junctions

Spin angular momentum transfer, or spin-transfer, describes the transfer of spin angular momentum between a spin-polarized current and a ferromagnetic conductor. The angular momentum transfer exerts a torque (spin-current induced torque, or spintorque) on the ferromagnetic conductor. When its dimensions are reduced to less than 100 nm, the spin-torque can become comparable to the magnetic damping torque at a spin-polarized current of high current density (above 10⁶ A/cm²), giving rise to a new set of current-induced dynamic excitation and magnetic switching phenomena. This has now been definitively observed in sub-100-nm current-perpendicular spin-valves and magnetic tunnel junctions, and appears promising as a basis for direct write-address of a nanomagnetic bit when the lateral bit size is reduced to well below 100 nm. An overview is presented in this paper of spintransfer phenomena. The first part of the paper contains a brief introduction to spin-transfer, especially the characteristic dynamics associated with spin-torque. In the second part, several representative experiments are described. In the third part, a set of basic phenomenological models are introduced that describe experimental observations. The models also serve as a bridge for quantitative comparison between experiments and first-principles spin-polarized transport theory. In the last part of the paper, some device concepts based on spin-transfer-induced magnetic excitation and magnetic reversal are described.

1. Introduction

It is well known that the configuration of magnetization orientation in a metallic ferromagnetic system affects the electron transport properties of the system. For example, in a multilayered magnetic and nonmagnetic metal thinfilm stack, the resistance of the stack depends on the relative magnetic orientation of the individual magnetic layers. The appreciable change in resistance resulting from this dependence came to be known as the "giant magnetoresistance" effect [1–4].

Spin angular momentum transfer, or spin-transfer, on the other hand, pertains to the reverse effect: the influence of a spin-polarized current on its host magnetic conductor, as depicted in **Figure 1**. Such spin-transfer-induced magnetization reversal is a relatively new phenomenon, and it is unambiguously observable only in magnetic structures smaller than $\sim 0.1~\mu m$ in size [5–10].

The phenomenon originates from the exchange of angular momentum between a spin-polarized current and the magnetization—a concept which has been developing over the years [11–17] that has led to the quantitative prediction of the spin-current-induced magnetization excitation and reversal [18] and its quantitative experimental verification [9].

A sketch for the basic concept of spin-transfer and its related macro-spin dynamics is shown in Figure 1. At the lower left in the figure is a two-ferromagnet layered spin-valve structure. The current passes through the left ferromagnet (F1) and becomes spin-polarized. When it passes through the second, thinner ferromagnet on the right (F2), the polarization direction of the current may have to change depending on the relative orientation of F2 and F1. This is illustrated at the upper left in the figure, where N designates a nonmagnetic conductor.

©Copyright 2006 by International Business Machines Corporation. Copying in printed form for private use is permitted without payment of royalty provided that (1) each reproduction is done without alteration and (2) the Journal reference and IBM copyright notice are included on the first page. The title and abstract, but no other portions, of this paper may be copied or distributed royalty free without further permission by computer-based and other information-service systems. Permission to republish any other portion of this paper must be obtained from the Editor.

0018-8646/06/\$5.00 © 2006 IBM

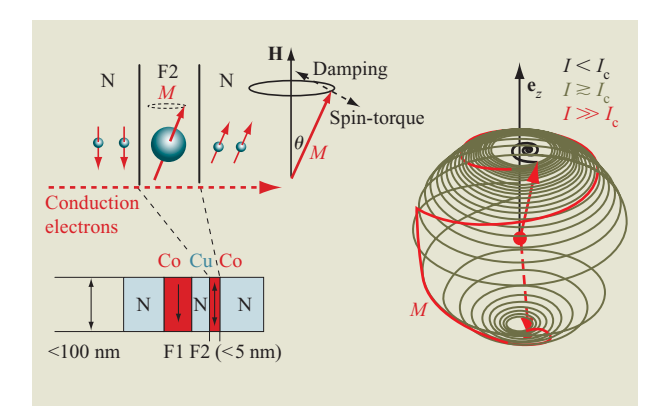


Illustration of spin-transfer and associated macro-spin dynamics. A uniaxial anisotropy is assumed to exist with its easy axis. The magnetic field ${\bf H}$ is applied in the same direction; M designates the magnetic moment of the ferromagnetic layer.

This "repolarization" process is what causes the second ferromagnet to experience an effective torque [18]. This spin-current-induced torque, or spin-torque, for the relative orientations illustrated here, is in a direction that opposes the magnetic damping torque for F2, as shown in the figure. For a large enough current, the spin-torque overcomes magnetic damping. This causes an instability to develop, and the precession cone angle increases over time. When the cone angle increases past the equator, both the damping torque and the spin-torque point toward the south pole, which becomes a stable point for F2, thus completing the magnetic reversal, as depicted at the right in the figure. The situation for reversed current direction is a bit more complex, but the net spin-torque on F2 remains proportional to the current. The reversal process remains essentially the same as the one described above [19, 20].

This new concept, the presence of a spin-torque on a ferromagnet due to spin-transport, affects our understanding of the magneto-transport problem on many levels. First, the process is microscopic and quantum-mechanical in nature, involving spin-polarized transport physics. The collective effect of the spin-transport is to present a net torque that can affect the magneto-dynamics of the ferromagnet. The magnetic response of the ferromagnet, in turn, would affect the electronic transport, making it a generally complex problem. Fortunately, for most physical systems, the electronic transport process and the magneto-dynamics operate on two very different time scales; this makes it possible to treat the transport and the magneto-dynamics processes separately, simplifying analysis.

The collective response of the magnetization in a ferromagnet is governed by the effective magnetic field through the well-known Landau-Lifshitz-Gilbert (LLG) dynamic equation [21] at a time scale that is usually greater than 100 picoseconds, depending on the anisotropy energy strength. For an isolated macro-spin, the time scale τ can be related to an effective magnetic field H, with the approximate relation $2\pi/\tau \sim 2\mu_B H/\hbar$, or about 0.5 nanosecond for every kilo-oersted of magnetic field. In the expression, μ_B is the Bohr magneton, and $\hbar = h/2\pi$, with h being Planck's constant. The spinpolarized electronic transport, on the other hand, tends to have a response time faster than or of the order of the spin-flip-scattering lifetime, which is of the order of several tens of picoseconds for materials with relatively little spin-flip scattering, such as Cu [22, 23], and shorter for materials with strong spin-flip scattering, such as Pt. The difference in these two time scales made it possible to mathematically simplify the problem. In treating the transport process, the moment of the ferromagnet can be assumed to be stationary in time. In treating the magnetic dynamics, the related adjustment for transport current can often be considered to be instantaneous. It is therefore possible to understand and summarize the microscopic spin-polarized transport process with a set of phenomenological parameters, and use the same set of parameters as inputs to model the slower dynamics of the magnetization.

The detailed relationship between the spin-torque of the spin-polarized current and that of the transport properties of the media the current is traversing is a quantum-mechanical transport problem that can be solved in several cases. The relationship depends on the specifics of the materials and interface arrangement as well as the nature of the transport current. The microscopic transport is not the main focus of this paper. Readers are referred to more advanced discussions presented in [17–20] and [24–27].

This paper focuses on the macroscopic consequences of the presence of a spin-torque. We first present a brief description of the magneto-dynamics for a macro-spin as it is driven by the spin-torque. We then survey recent experiments to highlight the important attributes of the spin-torque in its effect on magneto-transport and current-induced magnetic excitation. Among these are the presence of an instability threshold current; spin-transfer-induced magnetic reversal and persistent precession; amplified finite temperature thermal activation; the conservation of angular momentum; and the conservation of energy during the process. The macroscopic manifestation of the spin-torque connects the experimental findings with microscopic spin-dependent transport theory, and has led to

novel device concepts, some of which are discussed briefly at the end of the paper.

2. Basic macro-spin dynamics

A macro-spin model treats a nanomagnet with the assumption that its internal magnetic degrees of freedom are frozen. The only relevant parameters are the total magnetic moment \mathbf{m} and the magnetic anisotropy energy $U(\theta, \varphi)$, where θ and φ are the direction angles of \mathbf{m} . The shape of the nanomagnet is relevant only in that its related demagnetization energy contributes to the total anisotropy energy function $U(\theta, \varphi)$.

Dynamics of a nanomagnet under spin-currentinduced torque

When a spin-polarized current passes through a ferromagnetic electrode, the ferromagnet repolarizes the current in the direction of its magnetization. In the process, some of the angular momentum from the electron spins is absorbed by the ferromagnet, resulting in the exertion of a net torque (spin-torque) on the ferromagnet. A detailed analysis of the origin of this torque is given in [18] and references therein.

For a nanomagnet macro-spin within which the magnetization is uniform, the transverse component of the spin-torque is [18]

$$\Gamma = -g(\mathbf{n}_{m}, \mathbf{n}_{s})[\hbar(2e)](\eta I/m^{2})(\mathbf{n}_{s} \times \mathbf{m}) \times \mathbf{m}, \tag{1}$$

where \mathbf{m} is the magnetization vector, m is its magnitude, $\mathbf{n}_{\rm m}$ is its unit vector direction, $\mathbf{n}_{\rm s}$ is the direction of spinpolarization of the incoming current, and $\eta = (I_{\uparrow} - I_{\downarrow})/$ $(I_{\uparrow} + I_{\downarrow})$ is the spin-polarization factor, where I_{\uparrow} and I_{\downarrow} are the majority and minority spin-polarized currents with their polarization axis defined by the polarizing magnet (F1 in Figure 1). The term $g(\mathbf{n}_{m}, \mathbf{n}_{s})$ is a numerical prefactor that describes the angular dependence of the efficiency of spin-angular momentum transfer, originating from the quantum-mechanical nature of the interaction between spin-polarized current and the macro-spin; it may also depend on the global spin-current and the boundary condition of the spin-density [18, 19, 25]. The case of a constant $g(\mathbf{n}_{\rm m}, \mathbf{n}_{\rm s}) \equiv 1$ within the macrospinbased phenomenological model describes a simple redirection of the spin-current polarization direction and complete absorption of its transverse angular momentum by the macrospin. In reality, the detailed angular dependence of $g(\mathbf{n}_{m}, \mathbf{n}_{s})$ is model-dependent and is never an angle-independent quantity. Its macroscopic form in real materials systems has yet to be firmly established experimentally. For simplicity of discussion on a semiquantitative level, however, for now we assume a constant $g(\mathbf{n}_{m}, \mathbf{n}_{s})$, and use Equation (1) as the basic interaction that enters the magneto-dynamics equation for the motion of the macro-spin. The macrospin

dynamics can be phenomenologically described by the Landau-Lifshitz-Gilbert equation in the form

$$(1/\gamma)\frac{d\mathbf{m}}{dt} = \mathbf{m} \times \left[\mathbf{H} - (\alpha/m)\mathbf{m} \times \left(\mathbf{H} + \frac{\eta \hbar I}{2em\alpha} \mathbf{n}_{s} \right) \right], \quad (2)$$

where γ is the gyromagnetic ratio $g\mu_B/\hbar \approx 2\mu_B/\hbar$, and α is the LLG damping coefficient.

For dynamics studies including the internal degrees of magnetic freedom of the nanomagnet, Equation (2) can be viewed as a local constitution equation. Together with an exchange stiffness term, the vector field equation then describes the dynamics of the nanomagnet in the continuous medium limit. In a special case, the nanomagnet is a thin film with thickness much smaller than the lateral dimensions. In this case, the in-plane degrees of magnetic freedom can be taken into account by replacing $\mathbf{H} \to \mathbf{H} + (D/2\mu_{\rm B}) \nabla^2 \mathbf{n}_{\rm m}$, where $\nabla^2 = \partial_x^2 + \partial_y^2$ and x, y are the in-plane position coordinates, D is the exchange stiffness constant, and $\mathbf{n}_{\rm m} = \mathbf{M}/M$ is the local direction of magnetization at point (x, y).

Threshold current for magnetic amplification

For simple geometries and under a macro-spin approximation, Equation (2) can be linearized and solved for its stability boundary. For a thin free-layer nanomagnet in a collinear geometry with the easy axis of its uniaxial anisotropy field aligned with that of the applied field and the easy-plane anisotropy sharing its easy plane with the film plane, a stability threshold current I_c of

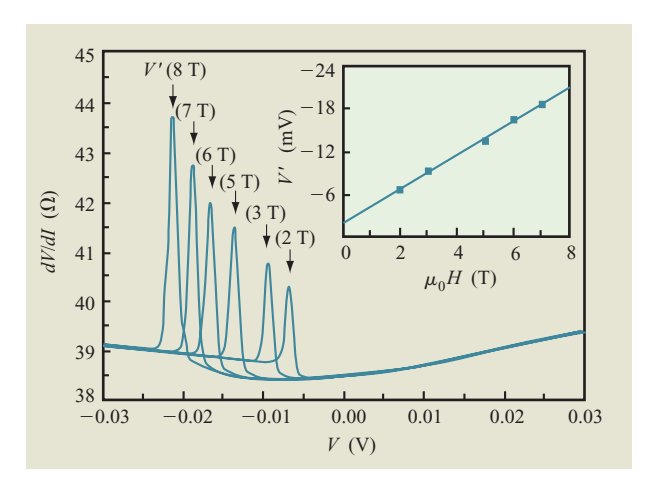
$$I_{\rm c} = \left(\frac{2e}{\hbar}\right) \left(\frac{\alpha}{\eta}\right) m \left(H + H_k + 2\pi M_{\rm s}\right) \tag{3}$$

is obtained [6, 18, 28]. Here M_s is the saturation magnetization of the free layer (F2), and $m = (abt)M_s$ is the total magnetic moment of the free layer, with a, b as its lateral dimensions and t as its thickness.

Equation (3) gives a current threshold above which the *linearized* LLG equation becomes unstable over time, and a net gain of the precession cone-angle results. In comparing with experimental results, however, effects of large cone-angle precession must often be carefully taken into account, since the development of an initial cone-angle increase dictated by the linear stability threshold may not necessarily lead to complete magnetic reversal [28]. However, in many simple systems such as those with uniaxial-only anisotropy or thin-film nanomagnets with a strong easy-plane anisotropy (due to demagnetization and a moderate in-plane uniaxial anisotropy), the linear stability threshold often leads to the reversal of the magnetic moment.

Several other factors affect the experimentally observable switching current. These are often significant;





Differential resistance of a point-contact junction formed by a silver tip and a Cu|Co|Cu|Co multilayer thin film. Inset: The threshold voltage (or current) depends linearly on the magnitude of the external magnetic field applied perpendicularly to the film surface. From [5], with permission; ©1998 American Physical Society.

the simple stability threshold expression [Equation (3)] does not account for them. Chief among these factors is the finite temperature effect. Other uncertainties include the relatively poor knowledge of the actual LLG damping coefficient for a particular device structure and of the exact spin-polarization value η . Details of the spin-transport, whether it is ballistic or diffusive, or knowledge of whether the interface contributes significantly to spin-flip scattering, can further complicate the picture. For simplicity, Equation (3) was derived using the extremely simplified spin-torque expression of Equation (1) with g=1. Detailed calculations for each of these specific spin-transport possibilities would give rise to additional angular dependences of the spin-torque as a function of the relative orientation between F1 and F2.

A simple way of comparing Equation (2) with experiment is to examine the intercept-to-slope ratio of the experimentally observed threshold boundary $I_{\rm c}(H)$, defined as $R_{\rm IS} = I_{\rm c}(0)/(dI_{\rm c}/dH)$. For Equation (3), $R_{\rm IS} = H_{\rm k} + 2\pi M_{\rm s}$. Experimentation on the other hand appears consistently to result in a lower value of $R_{\rm IS}$, by almost an order of magnitude, suggesting that additional mechanisms must be taken into account [29, 30].

One of the main causes for the experimentally measured decrease in $R_{\rm IS}$ well below $H_{\rm k}+2\pi M_{\rm s}$ is the finite temperature effect [30]. Equation (3) represents a zero-temperature stability threshold. At finite temperatures, additional thermal agitation is present,

making the apparent threshold current lower and yielding a smaller $R_{\rm IS}$ value.

Energy flow during precession and the Berger voltage

When the threshold current $I_{\rm c}$ is exceeded, precession at a large cone angle usually follows. Such large-cone-angle precession can cause an additional voltage rise across the spin-valve structure because of energy conservation. This can be accounted for as follows: The dissipation associated with magnetic damping is proportional to the square of the sine of the precession cone-angle. Hence, to maintain a large-cone-angle precession, energy must be supplied from the transport system, resulting in an additional voltage rise.

The presence of this dc voltage accompanying magnetic precession has been predicted by Berger [31]. For large-amplitude magnetic excitation in a highly asymmetric magnetic stack (where the free magnetic layer is much thinner than the thick layer), the asymptotic limit of the voltage rise due to precession is predicted to be $\Delta V(\omega) = (\hbar \omega/2e) (\sigma_1 - \sigma_2)/(\sigma_1 + \sigma_2)$, where $\sigma_{1,2}$ are the majority and minority channel conductivities defined by the thick ferromagnetic layer, corresponding to a spin-polarization factor of $(\sigma_1 - \sigma_2)/(\sigma_1 + \sigma_2) = (I_{\uparrow} - I_{\downarrow})/(I_{\uparrow} + I_{\downarrow}) = \eta$. Replacing $\omega = 2\mu_{\rm B}H/\hbar$ as the precession frequency gives

$$\Delta V = \eta \left(\frac{\mu_{\rm B}}{e}\right) H \,. \tag{4}$$

Equation (4) follows from energy conservation. To maintain the nanomagnetic precession at a cone angle θ , energy has to be delivered from the transport current to the magnetic system. This dissipation power, when supplied by a transport current of $I = I_c$, must give rise to a voltage difference ΔV , which gives $I_c \Delta V = -dU(\theta)/dt = \alpha \gamma m H^2 \sin^2 \theta$. For maximum spin-wave excitation, $\theta = \pi/2$, and hence $e(\Delta V) = \eta \mu_B H$. Here, $U(\theta) = -mH \cos \theta$.

Size consideration: Why spin-torque is most visible only in nanomagnets

There are two known mechanisms that can cause interaction between a magnetic moment and a transport current: current-induced magnetic field (the oersted field) and spin-polarized current-induced spin-torque. A current-induced magnetic field for a wire of radius r can be related to the maximum field (usually around the surface of the wire) and the current passing through the wire I. From Maxwell's equations, the relation is I = (c/2)rH (in gaussian units, c is the speed of light). A spin-valve of similar lateral size (2r) would have a spin-torque threshold current [following Equation (3)] of the order of $I_c \approx (H + H_k + 2\pi M_s)(4r^2t)M_s(\alpha/\eta)(2e/\hbar)$. The spin-torque threshold is proportional to r^2 , and the oersted-field-related current (for a given threshold field,

such as the anisotropy field $H_{\rm k}$) is proportional to r. Thus, at large dimensions the threshold from the oersted field is the lower threshold. The crossover point for highmoment thin films such as cobalt, with $H \sim H_{\rm k} \ll 2\pi M_{\rm s}$, is roughly

$$r_{\rm c} = \left(\frac{c\hbar}{4e}\right) \left(\frac{\eta}{\alpha}\right) \left(\frac{1}{M_{\rm s}t}\right) \left(\frac{H_{\rm k}}{2\pi M_{\rm s}}\right), \tag{5}$$

which gives, for 30-Å-thick cobalt, an $r_{\rm c}\approx 0.04~\mu{\rm m}$, assuming a spin-polarization factor of $\eta\approx 0.1$, an LLG damping coefficient $\alpha\approx 0.01$, and $H_{\rm k}\sim 100$ Oe. Thus, a practical crossover dimension for a pillar-structured spin-valve is of the order of $2r_{\rm c}\approx 0.1~\mu{\rm m}$, below which the spin-torque effect is more significant.

3. Early experimental evidence of spin-currentinduced magnetic excitation

Spin-current-induced magnetic excitation has been experimentally observed in many different systems. Earlier experiments [11–13], for example, illustrate the effect of the spin-angular momentum of a carrier on abrupt magnetic domain walls. Slonczewski [18] has predicted the presence of a spin-torque from a spinpolarized current in a magnetic multilayer geometry assuming ballistic transport and using WKB wave functions. More recently, experiments show currentinduced magnetic excitation in a point-contact junction on giant-magnetoresistance (GMR) multilayers [5, 7, 32], and magnetic switching in highly spin-polarized manganite junctions [6]. These experiments reveal the sometimes dramatic effect of the spin-torque, leading to the quantitative experimental observation of spintransfer-induced magnetic reversal [6] and the eventual unambiguous experimental demonstration [9] of the reversal and magnetic excitation effects in lithographically defined nanomagnet spin-valve junctions.

Tsoi et al. [5] have shown that magnetic excitation can result from bringing a point-contact tip made of silver into contact with a multilayered Cu|Co|Cu|Co · · · thin film. The current density under the point contact is high enough to exceed the spin-torque excitation threshold. As a consequence, a local excitation and reversal of magnetic moment results—probably only for the first cobalt layer. This manifests itself as a step in the current–voltage (I-V)characteristics of the point-contact junction, as shown in Figure 2. The threshold voltage (or current, since the junction is basically a linear resistor with only small nonlinear deviations) varies linearly with the magnetic field H, applied perpendicular to the film surface, and is large enough to overcome the easy-plane demagnetization field of cobalt (which is about $4\pi M_s \approx 17.6$ kOe). This linear dependence of threshold current vs. applied field is consistent with Equation (3). Another possible interpretation of this set of experimental data is the

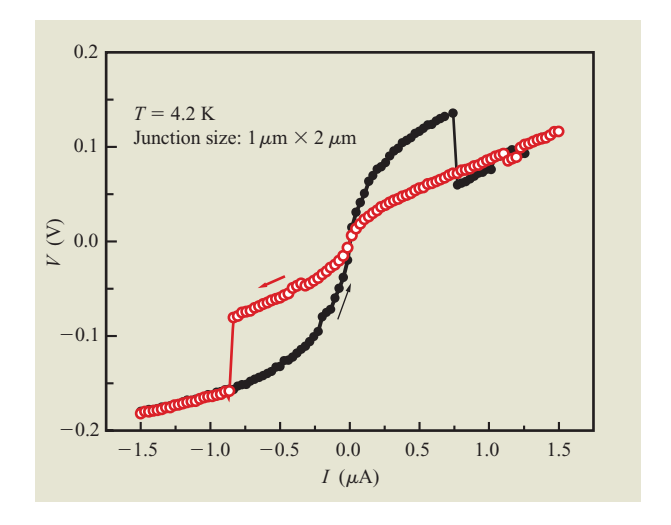


Figure 3

Example of the bias-current-induced switching of resistance in a ||LSMO|STO|LSMO|| trilayer junction. (LSMO is the Mn perovskite $\text{La}_{0.7}\text{Sr}_{0.3}\text{MnO}_3$; STO is the insulator SrTiO_3 .) The R_{high} and R_{low} values of the current-induced states correspond to those of the magnetic-field-induced R_{high} and R_{low} values. From [33], with permission.

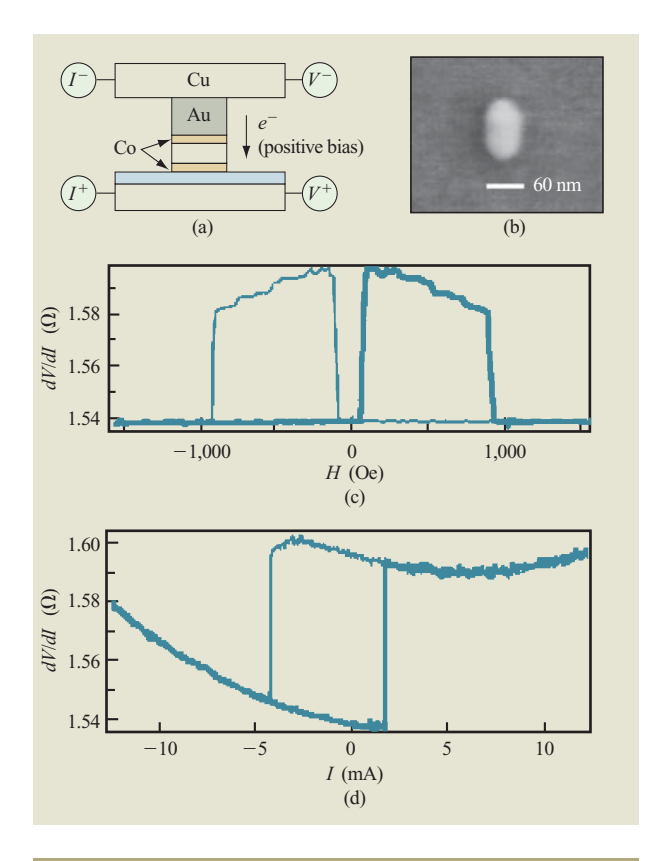
presence of a voltage threshold for spin-wave (magnon) emission at a certain energy, with the voltage threshold determined by the Zeeman splitting, $V_{\rm c} \approx (g\mu_{\rm B}/e)H$. Further discussion of the reason why these two apparently different interpretations may have some intrinsic relationship is given later.

Another form of the point contact onto magnetic layers was implemented by Myers et al. [7]. A special wafer with a SiN membrane was used, with a nanometer-size hole lithographically fabricated into the SiN membrane. The magnetic multilayers were then deposited on one side of the wafer, and the metal point contact (copper in this case) was deposited *in situ* on the other side, forming a metallic striction contact through the SiN hole and thus a point-contact junction. They observed not only signatures of magnetic excitation, but current-induced hysteretic magnetic reversal as well.

Earlier, current-induced magnetic reversal was observed in manganite-based all-oxide trilayer magnetic junctions such as the one shown in **Figure 3**. The junction was 1 μ m \times 2 μ m in size, although the actual current path was likely to be much smaller, perhaps of the order of several hundred angstroms.

We first observed this phenomenon in 1996. More systematic measurements of junctions with similar behavior were carried out later, indicating that the

¹ Unpublished work



Current-induced reversal of magnetization in a current-perpendicular spin-valve. The first definitive evidence of current-induced magnetic switching was obtained by Katine et al. [9] in 1999 using a structure similar to that shown here (a). The lateral size of the junction ranged from the earlier 120 nm or so in diameter [9] to the later geometry of 70 nm by 120 nm [34], as shown in the scanning electron micrograph (SEM) (b). The resistance vs. magnetic field sweep observed is shown in (c), and the resistance vs. bias current sweep observed is shown in (d). Resistance corresponds to dV/dI, which was measured using a lock-in detection method with an ac-bias current superimposed on the dc-bias current. From [34], with permission; ©2000 American Physical Society.

junction-switching behavior was consistent with a spin-transfer-induced magnetic reversal process [6, 33]. This experimental observation stimulated a renewed interest in the spin-angular momentum transfer process in spin-polarized transport systems. While large and dramatic at times, the transfer occurs in only a small fraction of the junctions prepared. Most likely it originates from interface-inhomogeneity-related current paths, and the switching occurs for only those junctions in which the interface inhomogeneity is at the right place with the right size. These particular junctions, while rare, switched with a well-defined threshold current [6], whose value showed a systematic dependence on applied magnetic field, in a

manner consistent with a simple spin-angular-momentum transfer model [6, 18].

Other experiments during this phase explored the interplay between spin-polarized current and the magnetic-field-driven reversal in nanomagnetic electrodes. An example was the work by Wegrowe et al. [8] in which an electroplated Ni wire, 80 nm in diameter and about 500 nm in length, was used. The work demonstrated a shift in the threshold magnetic field for a resistance-field hysteresis loop when a 10^7 -A/cm² pulsed current was present. The change of threshold field was about 100 Oe at a current pulse of 0.15 mA, larger than any induced magnetic field the current could generate. The authors argued that the spin-polarized current was affecting the magnetic reversal threshold field.

The quantitative proof of a spin-transfer-induced magnetic reversal was shown in 1999 for metal current-perpendicular (CPP) spin-valve nanomagnets by Katine et al. [9, 34]. They used electron-beam lithography to define a CPP spin-valve nano-pillar, about 100 nm in lateral dimension. An example of one such junction device is shown in **Figure 4**. A clear signature of magnetic reversal was observed at a threshold current density in the mid-10⁷-A/cm² range. The threshold current demonstrated the characteristic linear dependence on applied magnetic field, with a slope consistent with predictions based on the spin-transfer model [9, 34].

4. Lithographic fabrication of magnetic nanopillar spin-valve structures

Quantitative experimental investigation of the spin-transfer effect requires access to well-defined magnetic nanostructures of the order of 100 nm or less in lateral size. This is usually done using electron-beam lithography. Two strategies have been successfully used for the fabrication of spin-transfer devices with CPP structures: a substractive process and an additive process.

The subtractive process begins with a blanket multilayer film on a wafer with the intended CPP spin-valve layering structure formed as multilayers. Usually such multilayers are formed *in situ* in order to preserve the integrity of the thin-film interfaces. The interfaces are critical to spin-polarized transport and to the magnetic properties of the layers. The required CPP pillar-shaped structure is then formed by masked etching steps to remove certain parts of the films while preserving other areas, resulting in the desired device geometry. The process is based on the selective removal of materials—hence the term *subtractive patterning*.

Issues to consider in a subtractive process are the selectivity of the etching process between the mask material and that of the multilayer films forming the device. For magnetic metals, ion milling remains the most practical etching method, at least for laboratory

experiments. This is due in part to the difficulties involved in developing a reliable dry plasma etching process for ferromagnetic transition metals. In subtractive patterning, the magnetic multilayer stack must be prepared before going into the often lengthy and expensive lithographic process, making it a challenge to speed up the turnaround time necessary for materials development and optimization.

Such a process [35] is illustrated in **Figure 5**. The metal thin-film stack is formed first—with sputter deposition, for example. An e-beam resist such as PMMA [36] is used for the lift-off pattern transfer of 500 Å of Pt film which acts as a hard mask for subsequent ion-mill etching. Conventional photolithography is then used to form the base electrode structure. Ar ion milling is often used to transfer the pattern from the mask layer to film. An SiO₂ film is usually used for electrical isolation between the top and bottom electrode structures. Various etch-back and/or planarization processes for exposing the top contact of the junction have been explored.

The additive process uses a predefined structure on a substrate (such as a lift-off photoresist mask or a stencil mask of some other type) to define the necessary device structures. An example of a batch-fabricatable additive process developed in our laboratory [29, 37] is illustrated in **Figure 6**. The process shortens the cycle time between magnetic multilayer film deposition and final device testing. Moreover, because novel magnetic materials often are difficult to etch, a process allowing for controlled shape definition without having to etch magnetic thin films is also potentially more flexible.

Three types of thin films, Pt, Si, and Ge, have been successfully used as the masking layer, each having its own advantages and disadvantages. A Pt stencil is chemically more resilient, yet it is more difficult to etch. Ar ion milling often leaves uneven edges because the surface morphology of the Pt film reflects the underlying grain structure of the bottom electrode film. The use of Ge and Si stencils results in much better shape definition because there are well-developed dry-etch processes for them. However, their chemical stability is relatively poor against selective undercut SiO₂ etching, and could lead to long-term-storage-related stencil degradation and substrate contamination.

Examples of stencil structures formed by Pt and Ge are shown in **Figure 7**. Both were grown on a relatively thick (100–150-nm) copper base electrode.

CPP junctions have been fabricated [29, 37] with the stenciled substrate approach using both magnetron sputter deposition and electron-beam evaporation (e-beam evaporation). Magnetron-sputtered junctions showed more edge tapering [29] related to the larger spread in the incoming angle of the atomic beam. When deposited on a smoother bottom electrode (600-Å-thick

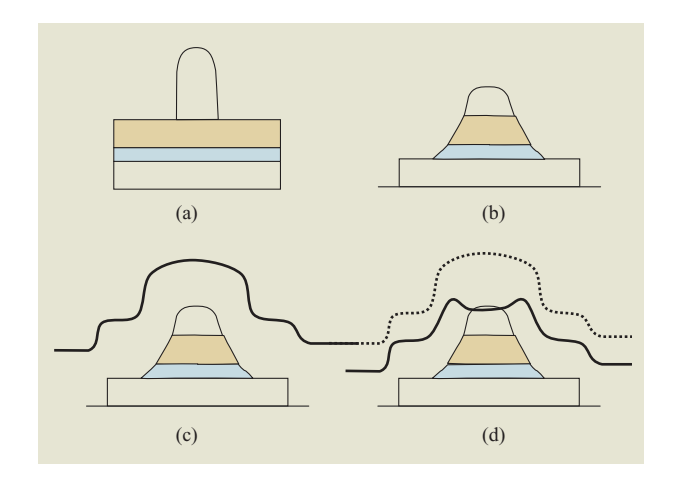


Figure 5

Example of a subtractive process: (a) Pt mask fabricated by lift-off of an e-beam-defined bilayer PMMA resist pattern. (b) The result of ion milling in order to transfer the metal mask pattern onto the junction stack. An optical lithography step is then used to define the base-electrode via (c) blanket coating of the entire structure with SiO_2 and "etch-back" in CF_4 of a (d) photoresist-planarized surface. The etching stops on the Pt, exposing the top of the junction for cross-wire contacting. This step makes use of the property that the photoresist etches at about the same rate as the SiO_2 . From [35], with permission.

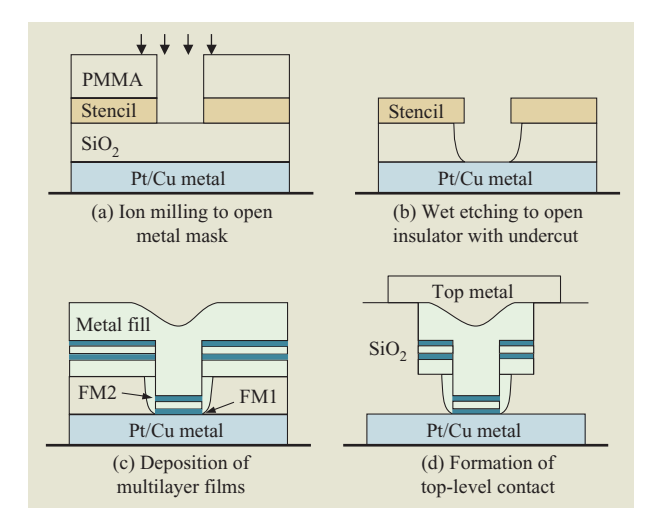


Figure 6

Schematic of the stencil process: (a) E-beam lithography and pattern transfer onto the stencil; (b) wet etching to open the insulator spacer and create a controlled amount of undercut; (c) deposition of magnetic stack followed by metallic filling to form top electrode contact; (d) optical lithography to define the wiring. Adapted from [29], with permission; ©2003 American Physical Society.

Scanning electron micrographs of illustrative stencils formed using (a) Pt and (b) Ge.

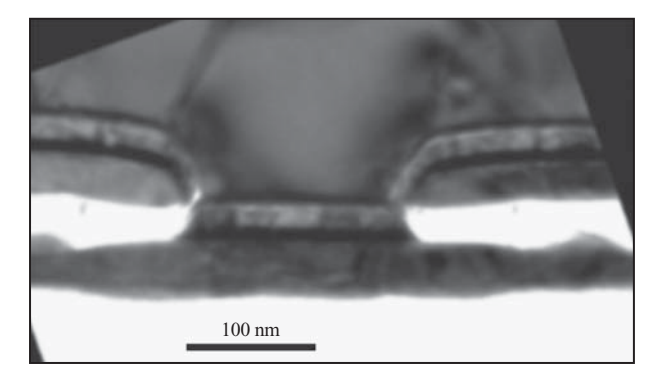


Figure 8

Cross-section transmission electron microscopy view of a sputtered magnetic tunnel junction, as described in the text. Courtesy of Prof. T. S. Kuan, State University of New York at Albany.

Pt layer), the individual layers forming the junction device could be clearly resolved, as shown in **Figure 8**.

After deposition of the layers forming the junction device, optical lithography was used to form the necessary electrodes.

5. Magneto-transport behavior of a spin-transfer junction

Quasi-static magnetoresistance properties

For a spin-valve-based magnetic junction, its magnetoresistance response to the combined effect of an applied magnetic field H and a bias current I shows three distinctively different response regions. They can be readily identified in the (I, H) parameter space.

Such magnetoresistance measurement is usually taken in a quasi-static setup (with measurement response time at 1 ms or less). A dc bias current is applied to the junction, and the junction resistance is usually measured by an ac-lock-in method (superimposing a small ac current above the dc bias). This method is particularly useful when the junction MR is only a small percentage of the resistance. In a typical quasi-static measurement in our laboratory, the bias current is stepped at a rate of approximately 0.2 to 2 mA/min, while the magnetic field sweep rate (if swept) is of the order of 500–1,000 Oe/min.

Generally speaking, the resistance response is hysteretic with respect to both applied field sweep and bias-current sweep. The values of the switching threshold current I^+ and I^- , corresponding to the resistance high-to-low-switching threshold and low-to-high threshold, are functions of the applied magnetic field and current history.

Figure 9 shows the hysteretic current and field dependence of the junction resistance. Parts (a) to (d) correspond to the sweeping of the bias current in both directions while the magnetic field is stepped, either up or down, between each bias-current sweep. The directions of the current sweeping and field stepping are indicated, respectively, by the vertical and horizontal arrows at the upper right corner of each part. Light color in the contour represents high resistance, dark color, low resistance. The magnetic spin-valve layer stack for this device was ||3Co|10Cu|12Co|200Cu|10Pt||. The numbers before the elements indicate the layer thicknesses in nm. This experimental switching-boundary phase diagram is not a simple stability boundary. It depends on the direction of the variables being swept and the history of the junction.

Generally speaking, there are three regions in these plots, as illustrated in **Figure 10**. The first region shows hysteretic switching between parallel and antiparallel states [note that the contour in Figure 10 corresponds to one set of switching thresholds, those represented by Figure 9(a)]. The second region shows a large amount of telegraph noise, often involving two-level fluctuations, signaling thermally activated transitions between two metastable states [38, 39]. These two states could be two orbits of persistent precession, they could be between two stable points, or they could be between one stable point and one orbit of persistent precession. In the third region

(high-field, high-current-density), a reversible step in the $V\!-\!I$ curve is seen. It appears as a peak in a dV/dI measurement; the peak has an amplitude and width that depend on the shape of the step as well as measurement conditions.

A direct correspondence between these quasi-statically measured R(H) phase diagrams and microwave emission characteristics has been established experimentally [40]. Most of the features observed can be found in mono-domain LLG models² [28, 41–43], since direct comparisons were made (between models and experimentally determined phase boundaries) in a magnetic field perpendicular to the junction film surface geometry [44].

More recent work has further probed the nature of dynamic excitation beyond the mono-domain limit [44], in general requiring numerical treatment of the LLG equation. Comparison of such numerical simulation (for example, see Lee et al. [45]) and experiment [40] gives satisfactory agreement to the leading order.

Time-dependent magnetoresistance during magnetic reversal

The response of a nanomagnet to spin-torque is dynamic. This can be investigated by time-resolved transport measurements. Such measurements also shed light on spin-torque switching time and its dependence on the conditions of the driving current, which is important for applications considerations.

Spin-transfer-induced magnetic reversal follows a different type of dynamics than those involved in magnetic-field-driven reversal. For present-day spin-valve devices, direct measurement of the switching speed of spin-transfer junctions is nontrivial because of the relatively small signal level involved. For CPP spin-valves, even at lateral sizes of 100 nm or less, junction resistance is still less than 10 Ω or so, and the magnetoresistance change is even smaller—usually only about 3–5% of the total junction resistance. This results in a MR-related voltage signal typically of the order of 0.1 mV. Dynamic calculations [28] indicate that the generic time scale of the reversal is approximately $(2\pi M_s)\gamma$. This estimate places the switching time in the range of about 1 to 10 ns.

Most switching dynamics measurements to date have been performed at ambient temperature. One earlier experiment probes the switching speed as a function of driving current amplitude [46]. Because of the small MR signal level above the large primary signal from the current step, an elaborate signal-averaging sequence was devised to extract the time-dependent evolution of the junction voltage related to magnetic reversal. With proper averaging, the output voltage difference can be

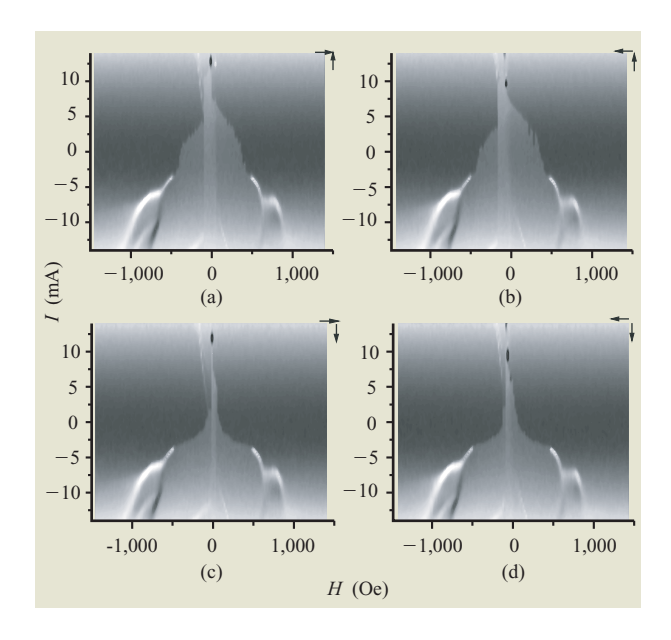


Figure 9

Contour plots of switching boundaries of a 0.05- μ m \times 0.10- μ m junction at ambient temperature. The magnetic field was applied along the easy-axis direction and the current was swept one full circle at a constant bias field. The bias field was then stepped to the next value. The vertical and horizontal arrows at the upper right corners of parts (a)–(d) respectively indicate the direction of current sweeping and field stepping. From [29], with permission; ©2003 American Physical Society.

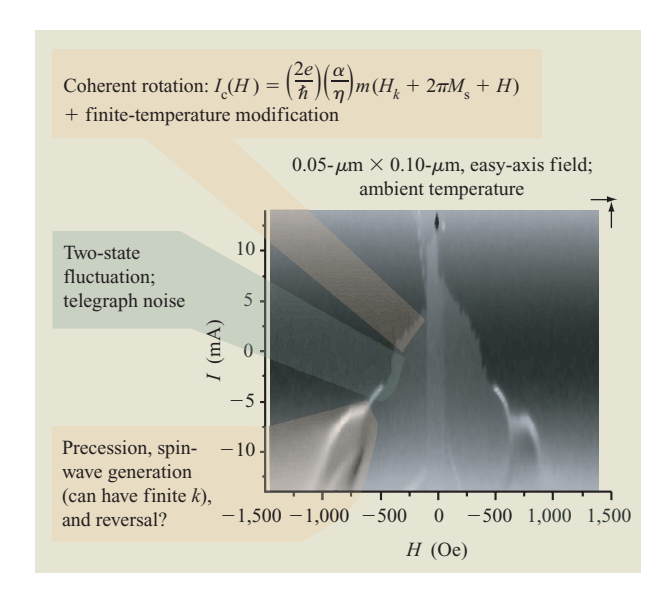


Figure 10

Three regions commonly seen for the spin-torque excitation of a CPP GMR nanojunction under current sweeping and field stepping.

² T. Valet, Grandis, Inc., Milpitas, CA, unpublished results, 2004.

(a) Time-dependent switching probability. (b) Switching speed τ^{-1} extracted from (a). Horizontal dashed lines with labels indicate the switching speed corresponding to a reversal time of 1 and 2 ns, respectively. (c) Switching speed plotted on a log-linear scale. The open and closed circles respectively represent the switching threshold on the positive and the negative current step of the junction. From [30], with permission.

normalized to reflect the ensemble-averaged reversal probability, as shown in Figure 11(a). The corresponding switching speed as a function of the drive current amplitude is shown on a linear scale in Figure 11(b), and on a log-linear scale in Figure 11(c).

Two aspects of the data obtained are shown in Figures 11(b) and 11(c). First, at the high speed limit, the dependence of τ^{-1} on bias current I is linear. Second, in the subthreshold, large-τ regime, the linearity gives way to a curved onset which is exponentially dependent on the bias current, as shown in Figure 11(c). The linear τ^{-1} vs. I dependence stems from spin-transfer angular momentum conservation, and the curved onset relates to thermal activation. Both can be adequately described by spintransfer dynamics in the presence of thermal noise. In addition, measured on the same sample under the same environment, the threshold current observed in Figure 11(b) was more than a factor of 2 larger than the corresponding threshold currents measured quasistatically. The difference between these two values lies in the vastly different time scales over which they were measured.

This experiment revealed only the envelope of the switching junction voltage response in time. The detailed oscillation in the voltage related to magnetic precession is sensitive to the initial condition, which is thermally randomized. It is therefore smeared out during trace averaging. A more recent experiment by Krivorotov et al. has revealed not only the envelope of the dynamic voltage output of the switching junction, but the actual oscillations that reflect the dynamic precession accompanying the reversal [47]. They achieved this by using a junction with a non-collinear magnetic moment arrangement between its fixed and free layers, introducing a distinctive initial condition for the precession dynamics upon the presence of a step-function driving current and thus preserving the phase information of the oscillations upon multi-trace averaging. In this way, they were able to observe the effect of spin-current on the damping characteristics of the nanomagnet by relating the oscillation envelope to the spin-current amplitude.

6. Finite-temperature macro-spin dynamics

A simple macro-spin finite-temperature dynamic model for spin-transfer-induced switching was first described in [30, 46]. The model captures the essential consequences of spin-transfer torque with an analysis of a collinear geometry between the direction of the macrospin and that of the spin-polarized current. A more detailed analysis of the model, based on Fokker–Planck equation formalism, can be found in [48, 49].

Review of the zero-temperature model

The model involves defining a macro-spin with its magnetic moment **m** with a direction described by a

unit direction vector $\mathbf{n}_{\rm m} = \mathbf{n}_{\rm m}(\theta, \, \varphi) = \sin \, \theta \, \sin \, \varphi \mathbf{e}_{x}$ $+\sin\theta\cos\varphi\mathbf{e}_{v}+\cos\theta\mathbf{e}_{z}$, where θ and φ are direction angles in a polar coordinate system. The moment \mathbf{m} is situated in a combined energy potential of $U = U(\theta, \varphi)$ which includes all energy-conserving torques that m comes to experience. The normalized gradient of U, expressed in terms of $\mathbf{H}_{\text{eff}} = (1/m) \nabla U(\theta, \varphi)$, includes the applied magnetic field H, a uniaxial anisotropy whose strength can be characterized by a uniaxial anisotropy field H_k , and an easy-plane anisotropy field that could be used to describe a macrospin in thin-film geometry experiencing the demagnetization effect from the flat thin-film geometry. The operator $\nabla = \mathbf{e}_{\theta}(\partial/\partial\theta) + \mathbf{e}_{\omega}(1/\sin\theta)(\partial/\partial\varphi)$, with unit vectors \mathbf{e}_{θ} and \mathbf{e}_{φ} respectively denoting the direction of rotation for θ and φ . Note that other than for an applied field H, H_{eff} is in general not a simple magnetic field vector but is instead a function of the angular position of m.

The precession dynamics of the macro-spin \mathbf{m} under a potential well U in the classical limit can be described by the phenomenological Landau–Lifshitz–Gilbert equation:

$$\left(\frac{1}{\gamma}\right)\frac{d\mathbf{m}}{dt} = \mathbf{m} \times \left[\mathbf{H}_{\text{eff}} - \left(\frac{\alpha}{m}\right)\mathbf{m} \times \mathbf{H}_{\text{eff}}\right]. \tag{6}$$

As was shown for Equation (2), adding the spin-torque term of Equation (1) gives

$$\left(\frac{1}{\gamma}\right)\frac{d\mathbf{m}}{dt} = \mathbf{m} \times \left[\mathbf{H}_{\text{eff}} - \left(\frac{\alpha}{m}\right)\mathbf{m} \times (\mathbf{H}_{\text{eff}} + \mathbf{H}_{\text{s}})\right], \tag{7}$$

where $\mathbf{H_s} = I\eta(\hbar/2e)(1/m\alpha)\mathbf{n_s}$ is the spin-angular-momentum transfer term. For simplicity, g=1 is assumed in using Equation (1).

If we examine the simple case in which only an applied magnetic field H is present in H_{eff} , and in which H and H_{s} are collinear, we obtain

$$\left(\frac{1}{\gamma}\right)\frac{d\mathbf{m}}{dt} = \mathbf{m} \times \left[\mathbf{H} - \left(\frac{\tilde{\alpha}}{m}\right)\mathbf{m} \times \mathbf{H}\right], \tag{8}$$

with $\tilde{\alpha} = \alpha + \hbar \eta I/(2emH) = \alpha(1+I/I_c)$, where $I_c = (2e/\hbar)(\alpha/\eta)(abtM_s)H_a$, a special case of the threshold current defined in Equation (3). This reveals the role of the spin-polarized current I: It modifies the effective damping coefficient of the nanomagnet. When α becomes negative, the nanomagnet amplifies disturbances away from its equilibrium position, resulting in a magnetic instability and then a magnetic reversal.

For more general situations, since \mathbf{H}_{eff} contains the angular position $(\theta,\,\phi)$ of \mathbf{m} , a full stability analysis of Equation (7) is required. This in small cone-angle limit $(\theta\ll\pi)$ can be done analytically with a linearized Equation (7), as was done in [9, 18, 24, 28]. When averaged over a time scale longer than the natural

precession period $\Omega_{\rm K}=\gamma H_{\rm K}$, it gives an effective damping coefficient of $\tilde{\alpha}=\alpha+\hbar\eta I/[2em(H+H_{\rm k}+2\pi M_{\rm s})]$ that describes the average cone-angle evolution $\langle\theta(t)\rangle$. Here the uniaxial anisotropy field $H_{\rm k}$ and the orthogonal easy-plane anisotropy term are included. If a thin-film demagnetization-related easy-plane anisotropy energy is assumed to apply, $M_{\rm s}=m/v$, where v=abt is the volume of the nanomagnet. When $\tilde{\alpha}=0$, the resulting instability threshold is characterized by Equation (3): $|I_{\rm c}|=(1/\eta)(2e/\hbar)m\alpha(H+H_{\rm k}+2\pi M_{\rm s})$. This threshold current $I_{\rm c}(H)$ depends linearly on the applied field H. It should have an intercept-to-slope ratio of $H_{\rm k}+2\pi M_{\rm s}$. However, experimental results [29] suggest that the actual slope-to-intercept ratio falls well below this, and the finite-temperature effect plays an important role.

The effect of finite temperature on the response of the macro-spin system to a spin-transfer excitation is twofold. First, it affects the average precession motion of the macro-spin by adding thermal agitation, resulting in finite probabilities for thermal activation over the magnetic energy barrier. Second, it adds a thermally distributed initial condition to the macro-spin.

Finite-temperature LLG equation

By following the approach of Brown [50] and of Grinstein and Koch [51], a Langevin random field \mathbf{H}_{L} can be added to the effective magnetic field term $\mathbf{H}_{\mathrm{eff}}$. The field \mathbf{H}_{L} relates to the system temperature T as $H_{\mathrm{L},i} = \sqrt{2\alpha k_{\mathrm{B}}T/\gamma m}I_{\mathrm{ran},i}\left(t\right), (i=x,y,z)$, where $I_{\mathrm{ran}}(t)$ is a gaussian random function with the first two moments of $\langle I_{\mathrm{ran}}\left(t\right)\rangle=0$ and $\langle I_{\mathrm{ran}}^{2}\left(t\right)\rangle=1$. Each of the x,y,z components has its own uncorrelated $I_{\mathrm{ran}}(t)$. Without the spin-transfer effect, the finite-temperature LLG equation with a Langevin random field reduces to

$$\left(\frac{1}{v}\right)\frac{d\mathbf{m}}{dt} = \mathbf{m} \times \left[\mathbf{H}_{\text{eff}} + \mathbf{H}_{\text{L}} - \left(\frac{\alpha}{m}\right)\mathbf{m} \times \mathbf{H}_{\text{eff}}\right], \tag{9}$$

which describes the dynamics of a macro-spin \mathbf{m} in a potential well $U(\theta, \varphi)$, with a thermally activated motion and a finite lifetime (with respect to remaining in the potential well), namely a thermally activated lifetime τ approximately following the Boltzmann statistics of

$$\tau = \tau_0 \exp\left(\frac{\Delta U}{k_{\rm B} T}\right) \,, \tag{10}$$

where ΔU is the potential barrier height as seen from the local minimum around which **m** fluctuates, and $\tau_0 \sim 1/\gamma H_{\rm k}$ is the reciprocal attempt frequency. Equation (9) should apply when $\Delta U/k_{\rm B}T\gg 1$. The lifetime τ is determined once a system is defined by Equation (9), and the energy landscape $U(\theta,\,\phi)$ is represented in Equation (9) by $\mathbf{H}_{\rm eff}(\theta,\,\phi)=(1/m)\mathbf{V}U(\theta,\,\phi)$.

Finite-temperature LLG equation with spin-torque: Amplified thermal activation

Spin-transfer excitation adds an additional torque. Similarly to Equation (7), after the spin-transfer torque is included, and assuming that the spin-polarized current carries no entropy flow into the macro-spin, Equation (9) becomes

$$\left(\frac{1}{\gamma}\right)\frac{d\mathbf{m}}{dt} = \mathbf{m} \times \left[\mathbf{H}_{\text{eff}} + \mathbf{H}_{\text{L}} - \left(\frac{\alpha}{m}\right)\mathbf{m} \times (\mathbf{H}_{\text{eff}} + \mathbf{H}_{\text{s}})\right], (11)$$

with H_s representing the spin-transfer-torque-related contribution, as defined in Equation (7).

It is instructive to examine the case in which \mathbf{H}_s and \mathbf{H} are both collinear to the easy axis of the uniaxial anisotropy term \mathbf{H}_k inside \mathbf{H}_{eff} and the easy-plane anisotropy is zero. In this case, and for small cone-angle $\theta \ll 1$, the effect of \mathbf{H}_s is simply to modify $\mathbf{H}_{eff} \to \tilde{\mathbf{H}}_{eff} = (H_k + H + H_s)\mathbf{n}_s = H_k + H)[1 + H_s/(H_k + H)]\mathbf{n}_s = [1 + H_s/H_k + H)]\mathbf{H}_{eff}$. Thus, one is able to rewrite Equation (11) in the form of Equation (9):

$$\left(\frac{1}{\gamma}\right)\frac{d\mathbf{m}}{dt} = \mathbf{m} \times \left[\mathbf{H}_{\text{eff}} + \mathbf{H}_{\text{L}} - \left(\frac{\tilde{\alpha}}{m}\right)\mathbf{m} \times \mathbf{H}_{\text{eff}}\right], \quad (12)$$

where $\tilde{\alpha} = [1 + H_s/(H_k + H)]\alpha = (1 + I/I_c)\alpha$, with $I_c = (2e/\hbar)(\alpha/\eta)(abtM_s)(H + H_k)$, another special case of Equation (3).

Equation (12) is a mathematically equivalent description of the same macro-spin system as that given in Equation (9) with the same amplitude of \mathbf{H}_{L} . This then suggests that $H_{\mathrm{L},i} = \sqrt{2\alpha k_{\mathrm{B}}T/\gamma m}I_{\mathrm{ran},i}(t)$ remains valid for this case—however, with the damping coefficient α replaced by $\tilde{\alpha}$. To maintain $H_{\mathrm{L},i}$, the macro-spin would have to experience a fictitious temperature \tilde{T} , such that $\tilde{\alpha}\tilde{T} = \alpha T$.

Since Equation (12) is equivalent to a macro-spin at temperature \tilde{T} with damping $\tilde{\alpha}$, one may further deduce that the thermal activation lifetime of the system can also be expressed in the form of Equation (10), except with its temperature rescaled to \tilde{T} . That is,

$$\tau = \tau_0 \exp\left(\frac{\Delta U}{k_{\rm B}\tilde{T}}\right) = \tau_0 \exp\left[\frac{\Delta U}{k_{\rm B}T}\left(\frac{\tilde{\alpha}}{\alpha}\right)\right]$$

$$= \tau_0 \exp\left[\frac{\Delta U}{k_{\rm B}T}\left(1 - \frac{I}{I_{\rm c}}\right)\right]. \tag{13}$$

Such linear behavior with I can be directly compared with experiments carried out at a subthreshold driving current $(|I| < I_c)$.

A more rigorous theoretical treatment that results in Equation (13) has been described by Li and Zhang [48]. The energy distribution of a macro-spin under spin-current excitation has been calculated by Apalkov and Visscher [52].

Thermally distributed initial condition

In the simple collinear geometry, the initial condition of the macro-spin system under spin-transfer excitation is most important when the spin-transfer excitation is large, for example when it approaches or exceeds the zero-temperature threshold current I_c . In this case, when the spin-transfer current is applied suddenly (at time t_0), it should result in a fairly rapid magnetic reversal. The switching time required at zero temperature is estimated [29] to be

$$\begin{split} \tau^{-1} &= \frac{\alpha \gamma}{m \ln{(\pi/2\theta_0)}} (H + H_{\rm k} + 2\pi M_{\rm s}) \left[(I/I_{\rm c}) - 1 \right] \\ &= \frac{\eta \left(\mu_{\rm B}/e \right)}{m \ln{(\pi/2\theta_0)}} (I - I_{\rm c}) \quad (I > I_{\rm c}), \end{split} \tag{14}$$

with θ_0 being the initial deviation of **m** from its easy-axis direction. The second line in Equation (14) reveals angular momentum conservation. At a finite temperature, θ_0 is thermally distributed. Thus, the precise switching speed varies from measurement to measurement. At the same time, the thermal agitation during the course of reversal adds some uncertainty to the exact speed and trajectory of the reversal. This disturbance is likely to be small compared to the large cone-angle motion involved in these reversal events as long as $\Delta U/k_BT\gg 1$.

To illustrate the consequences of a thermally distributed initial θ_0 , we examine a special case with $U(\theta, \varphi) = K (\sin^2 \theta + h_p \sin^2 \theta \cos^2 \varphi - 2h \cos \theta)$, where $K = mH_k/2$ is the uniaxial anisotropy energy constant, $h_p = 4\pi M_s/H_k$ is the easy-plane anisotropy field in dimensionless units, and $h = H/H_k$ is the applied field, assuming a collinear geometry between **H** and **H**_k. Furthermore, we assume that the thermal fluctuation amplitude is small when $\xi = K/k_BT \gg 1$. In such a limit, the main effect of finite temperature on the delay τ is through the initial angular position of θ , which in the limit of $K/k_BT \gg h_p \gg 1$ gives a switching speed based on the ensemble-averaged switching time [30]:

$$\langle \tau \rangle^{-1} \approx \frac{\eta \mu_{\rm B}}{me} \left[\frac{\ln (4\pi^2 h_{\rm p})}{\pi \ln (K/K_{\rm B}T)} \sqrt{\frac{1+h}{h_{\rm p}}} \right] (I - I_{\rm c}).$$
 (15)

In this particular limit, the ensemble-averaged switching speed has a current dependence with a slope that is directly dictated by the thermal-activation-induced initial angle. This is true only if no transient disturbance fields are present during the application of the current pulse. Such transient fields would create a sudden rotation of the effective easy-axis direction, in effect creating a non-zero and non-thermal initial angle θ_0 and thus dictating the speed of spin-transfer switch.

Summarizing the temperature-dependence results discussed so far, we conclude the following:

$$\langle \tau \rangle^{-1} \approx \begin{cases} \tau_0^{-1} \exp \left[-\frac{K}{k_{\rm B}T} (1-h)^2 \left(1 - \frac{I}{I_{\rm c}} \right) \right] & \text{when } (I \ll I_{\rm c}), \\ \left(\frac{\eta \mu_{\rm B}}{me} \right) \left[\frac{\ln{(4\pi^2 h_{\rm p})}}{\pi \ln{(K/k_{\rm B}T)}} \sqrt{\frac{1+h}{h_{\rm p}}} \right] (I - I_{\rm c}) & \text{when } (I \gg I_{\rm c}). \end{cases}$$

$$(16)$$

Equation (16) describes the experimental observation presented in Figure 11: a linear dependence of switching speed and drive current amplitude above a switching threshold current I_c , and a log-linear dependence below the threshold.

The slope of switching speed vs. drive current reflects angular momentum conservation. The product $(I-I_{\rm c})\langle \tau \rangle$ is also an important figure of merit for the possible application of a spin-current-driven magnetic switch as a memory element.

Recently two other experiments have revealed a similar set of relationships between the pulse-width and pulse-height dependence for such a switch [53, 54]. A generally similar behavior is reported, although these experiments measure the magnetic switching probability in the long-time limit, including switching events that may occur after the removal of the pulsed driving current. Therefore, the statistics for the switching probability of the nanomagnet should be somewhat different from those for Equation (16).

7. Spin-wave excitation and microwave emission

Spin-transfer-induced magnetic excitation can result not only in transient magnetic precession and reversal, but in persistent magnetic precession as well, and hence in the emission of spin-waves. Spin-wave excitation in the presence of a nanometer-scale patterned boundary confinement results in discrete modes [55]. This may be responsible for much of the complex behavior seen in the reversible (I, H) region [29], such as the behavior depicted in Figure 9. Spin-wave excitation can occur in magnetically confined nano-pillar spin-valve geometries [40], or possibly in magnetically extended structures in which the magnetic film under excitation is extended in nature and the transport charge current is confined by the arrangement of electrodes (for example, as in a pointcontact junction [5] or a lithographically prepared normal metal pillar in contact with an extended magnetic film structure [56-59]). These types of structures have been successfully prepared and associated spin-wave emission from spin-current demonstrated, in some cases unambiguously through the direct observation of microwave output spectra as a function of junction

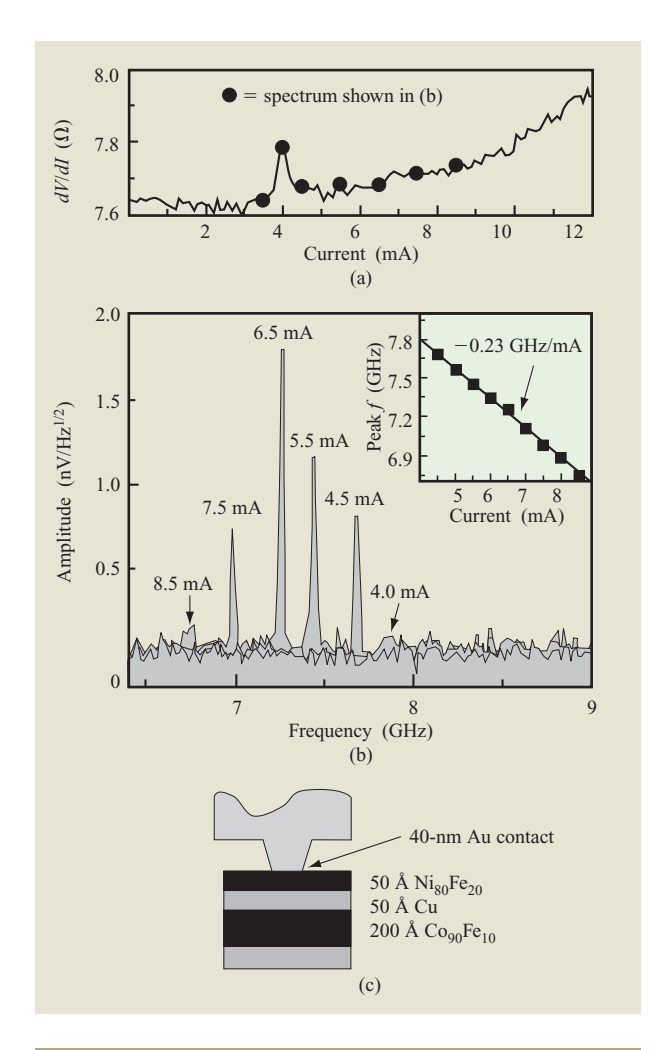
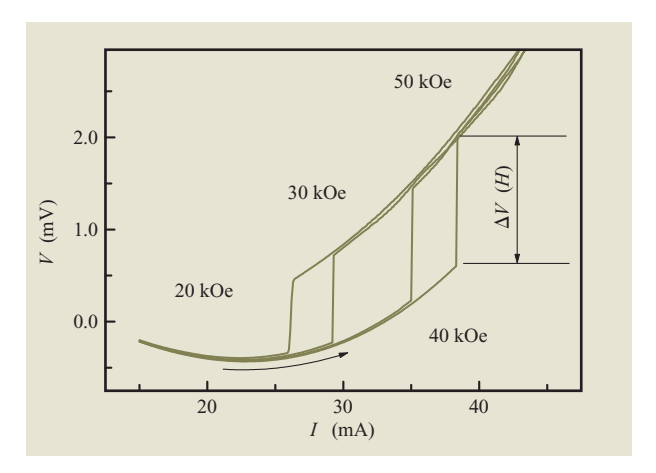


Figure 12

Microwave emission from spin-current excitation in nano-contact junctions: (a) Section of the *I–V* curve of a junction from which such emission is measured. (b) Microwave power spectra as a function of bias current, with inset showing the dependence of frequency on the bias current. (c) Geometry of the junction. Parts (a) and (b) reproduced from [56], with permission; ©2004 American Physical Society.

current and magnetic field bias [40, 56]. **Figure 12** gives an example of one such measurement. The junction used in this measurement was fabricated via a magnetic stack of $||2.5\text{Ta}|50\text{Cu}|20\text{Co}_{90}\text{Fe}_{10}|5\text{Cu}|5\text{Ni}_{80}\text{Fe}_{20}|1.5\text{Cu}|2.5\text{Au}||$. The magnetic layers were continuous, whereas the contact was about 40 nm in diameter at its upper surface.

The process of spin-wave excitation in isolated nanomagnetic pillar structures can be reasonably well modeled by a macro-spin model [40, 44], although magnetic excitations of finite wavelength comparable to the lateral dimension of the structure are also likely to be present.



I-V characteristics measured for a 0.05- μ m \times 0.20- μ m CPP junction. A linear background of 0.935 Ω is subtracted from the data to make the threshold behavior clearly visible. The characteristics shown are for applied field values of 20, 30, 40, and 50 kOe. The curvature is commonly seen for CPP junctions, and is believed to be the result of joule heating. The arrow shows the direction of current sweep. The data were obtained at 5 K. From [62], with permission; ©2005 American Physical Society.

Spin-wave excitation of an extended magnetic film under a localized point-contact spin-current excitation has previously been examined theoretically [24], resulting in an analytical solution. The spin-wave produced was shown to have a half-wavelength about the size of the point contact, resulting in a threshold current that was essentially independent of the contact area. Experimental work using mechanical point contacts to bilayers of magnetic thin film was found to be in semi-quantitative agreement with predictions [57]. A controlled junctionarea dependence (or independence) of the switching threshold current remains to be shown experimentally.

At a high current density, the internal magnetic degrees of freedom of the nanomagnet become very important because energy can be directed into spin-wave modes of different wavelengths. Full micromagnetic modeling is necessary to understand the large-amplitude behavior in this region [45]. The basic features between experiment [40] and full micromagnetic modeling [45] appear to agree with each other. Details of the particular spin-wave modes excited would depend not only on device design but on other subtle features of the magnetic boundary conditions of the nanomagnet, such as associated shape and materials irregularities formed during fabrication.

One piece of important information one can extract from such spin-wave excitation measurements is the

magnetic-field dependence of the threshold current, dI_c/dH . For a quantitative comparison of this quantity with model calculation, the junction sample is placed in a magnetic field which is applied perpendicularly to the film surface and is large enough to overcome the thin-film-shape-related demagnetization field $4\pi M_s$ (which for cobalt is about 17 kOe). The use of such a large field also has the added benefit of making finite-temperature fluctuation much less of an issue, at least within the approximation of a macrospin model. The penalty for such a measurement arrangement is the large amount of spin-polarized current that will be necessary to excite the appropriate magnetic precession and/or reversal because the applied magnetic field involved is relatively large.

8. High-field response and constraints on signal voltage amplitude

Experimentally, a spin-valve nanomagnet junction under a strong, perpendicular applied magnetic field exhibits two main characteristics. First is the presence of a (often non-hysteretic) voltage step at a certain bias current, as shown in Figure 13. Second, the voltage step height is seen to be similar to both the Zeeman-energy-related voltage $(\hbar\omega/2e)$, where $\hbar\omega\approx g\mu_{\rm B}H$ corresponds to the ferromagnetic precession frequency, and the giantmagnetoresistance-related voltage associated with a magnetic reversal, $V_c \sim I_c \delta R$, where δR is the resistance change of the junction between the magnetically parallel and anti-parallel states and I_c is the position of the current step. This is illustrated by the data shown in Figure 14. These observations have been interpreted either as a consequence of magnetic reversal of the free layer [60], or as a result of magnon-emission-related magnetic excitation [61]. However, this "coincidental" similarity between the observed voltage step height with $\hbar\omega/2e$ and with $V_{\rm c}\sim I_{\rm c}\delta R$ remains a tantalizing puzzle.

This similarity has been seen over many samples and from results obtained by many different groups. A summary of the experimental observations is given in **Table 1**. A recent study [62] suggests that this may be not a simple coincidence after all, and may indicate that the spin-valves are within the limit of spin-pumping-dominated dissipation [63, 64]. Spin-pumping-induced dissipation provides an additional relationship between the MR of a spin-valve and that of the spin-torque threshold current I_c , leading to the relationship $I_c \delta R \sim (2\mu_B/e)H$.

This conclusion, if verified by more rigorous theoretical analysis and experimental investigation, may place an order-of-magnitude estimate on the maximum amount of signal voltage that can be expected from a spin-valve-based junction under spin-current-driven magnetic reversal, independently of the impedance of the junction device. This is especially true when the objective is to

minimize the switching current threshold while maximizing signal voltage output.

9. Potential applications

Spin-transfer-induced magnetic excitation and magnetic reversal is a relatively new phenomenon that begins to dominate magnetic behavior for junction devices below about 0.1 to 0.2 μ m in lateral size. As the critical dimensions of current electronic devices shrink below this length scale, the spin-transfer mechanism becomes important in several aspects. It may be used for localized write-addressing of a magnetic random memory element, or for on-chip generation of tunable microwave radiation. The mechanism may also have a significant impact on the design and operation of magnetic disk read heads.

A two-terminal spin-valve or magnetic tunnel junction that can be current-switched between two stable resistance states constitutes a memory element. For such a memory element to be integrated into the existing CMOS circuit technology, some basic device requirements must be met. Chief among them are those that pertain to device impedance, device voltage swing between the two stable states, and threshold current required to switch the device. Switching speed and its relationship and tradeoff with switching current are also important.

To achieve effective integration, the current density required for device switching must be comparable to that supplied by a typical CMOS circuit of comparable density. If this were to be supplied by a MOSFET transistor, it would usually be of the order of 0.5 to 1 mA/µm of channel width. This determines the upper limit of the switching current. Diode selection could in principle allow for higher current density, although there are additional concerns regarding associated impedance (mis)match and uniformity of device characteristics over large numbers of junctions and diodes.

The other constraint on the junction switching current is that it must be large enough to switch a nanomagnet that has sufficient thermal stability to retain its remanent state at room temperature. This requires a magnetic anisotropy energy $U_k = (1/2)mH_k$ of the order of 40 to $60k_BT$. The high-speed switching threshold current I_c in Equations (16) and (3) can be directly related to this uniaxial anisotropy energy in the form [6, 28] of $I_c \approx (2e/\hbar)(\alpha/\eta)U_k$. Depending on the values of the damping α and spin-polarization factor η , this gives $I_c \approx 10$ –100 μ A for $U_k \approx 60k_BT$.

Present-day spin-transfer switching junction devices typically involve a quasi-static switching current of the order of 0.1–1 mA for a device cross section size of approximately 50–100 nm, resulting in a quasi-static switching threshold current density of the order of

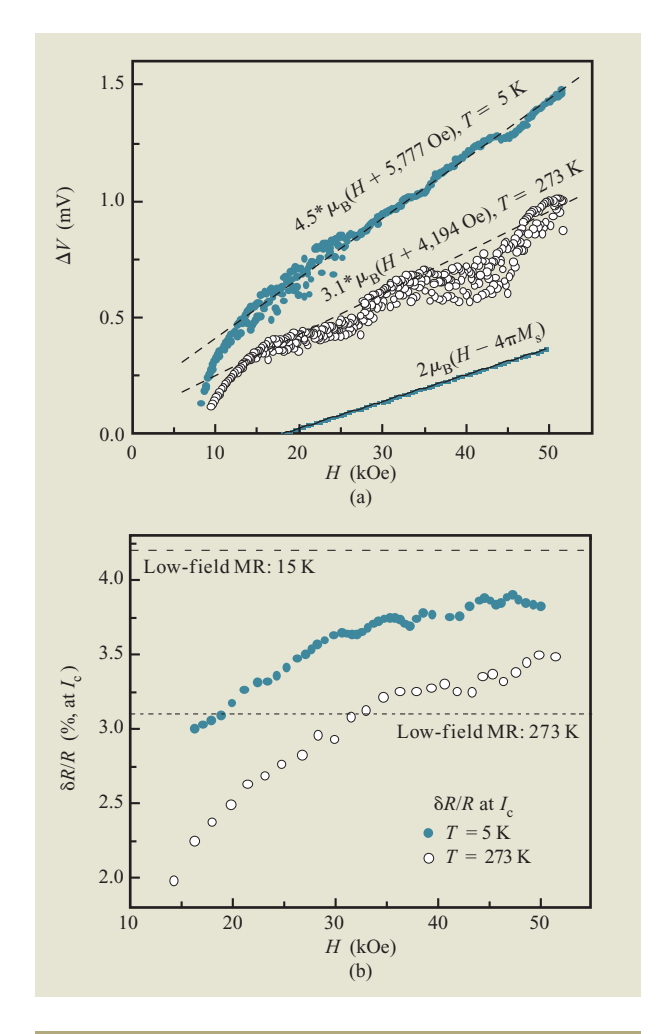


Figure 14

(a) Magnetic field dependence of ΔV at threshold current I_c , from Figure 13. The threshold current and ΔV at that current increase with the applied magnetic field. For comparison, the solid line on the bottom is the voltage corresponding to the Zeeman energy $(2\mu_{\rm B}/e)~(H-4\pi M_{\rm s})$. (b) The apparent resistance change at a critical current I_c (H) defined as $\delta R/R$, where $\delta R=\Delta V/I_c$. The dashed lines indicate low-field R(H) measurement-based MR at 15 K and 273 K.

10⁶A/cm². To be useful for CMOS integration, at least another order of magnitude reduction would be necessary. The high-speed switching threshold, as shown earlier, can be significantly higher (by perhaps a factor of 2–5 depending on device structure details).

Existing low-impedance (1 to $10 \Omega/\mu m^2$) magnetic tunnel junctions can support a transport current of the order of 10^7 A/cm^2 before inducing a barrier-related breakdown. Such current density is sufficient to demonstrate spin-transfer effect. The long-term stability and feasibility of integration with CMOS drive circuitry are yet to be demonstrated.

Junction stack	Lateral size (nm × nm)	δR (Ω)	$dI_{\rm c}/dH$ (A/Oe)	$(dI_{\rm c}/dH)$ δR	Т (К)	Ref.
120Cu 10Co 6Cu 2.5Co 15Cu 3Pt 60Au	100×100	0.075	2.90×10^{-7}	3.76	300	[9]
10Cu 3Co 10Cu 12Co 300Cu 10Pt	90×140	0.03	4.51×10^{-7}	2.34	4.2	[60]
80Cu 40Co 10Cu 3Ni80Fe20 2Cu 30Pt	70×130	0.129	2.16×10^{-7}	4.82	4.2	[44]
150Cu 20Pt 10Cu 2.5Co 10Cu 12Co 250Cu 10Pt	50×200	0.039	4.80×10^{-7}	3.23	5	[62]

A large part of the threshold current of a presentday spin-transfer device comes from the easy-plane demagnetization field due to its thin-film geometry. This type of anisotropy does not contribute to thermal stability, and yet, since the spin-transfer excitation involves significant out-of-film-plane precession, this easy-plane anisotropy significantly increases the spintransfer switching current. Therefore, one possibility for reducing the switching current of a spin-transfer device is to reduce or eliminate this easy-plane anisotropy from the system. This could possibly be achieved by careful engineering of the interface magnetism of the free layer or control of its stress field (for materials with a large magnetostriction coefficient). Although these possibilities are theoretically feasible, significant materials and fabrication challenges would have to be overcome before they could be successfully implemented in a manufacturable fashion.

The threshold current, as expressed in relations such as Equation (3), provides only an order-of-magnitude estimate for the switching current necessary for memory circuit operation. To achieve sufficiently rapid switching, the drive current would have to be greater than the threshold current, perhaps by a significant amount. The switching-speed vs. switching-time tradeoff is well captured by the curves presented in Figure 11. It is the linear slope in front of the second equation in Equation (16). For the 50-nm \times 100-nm \times 3-nm cobalt nanomagnet of Figure 11, the figure of merit for $(I-I_c)\langle \tau \rangle$ was about 8 pC.

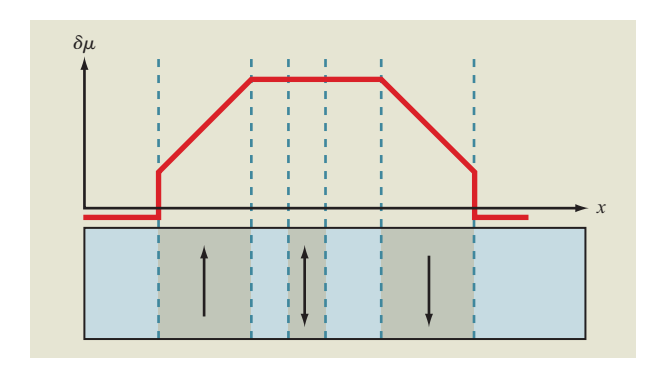
For finite-temperature operation as a memory element, the collinear switching geometry is unlikely to be the best, because for that geometry the initial condition of the switch depends sensitively on the thermal distribution. A non-collinear arrangement between the orientation of the "free" layer of the nanomagnet and that of the spin-polarized current is more desirable. At the same time it may be helpful through layout design to add a current-induced magnetic field as a transient "tipping" field in order to create a non-equilibrium initial state when switching the nanomagnet.

In addition to possible applications as a bi-stable resistor for memory circuits, spin-transfer devices have also been explored for potential use as compact, on-chip microwave oscillators [56]. Experiment has demonstrated tunable microwave output from spin-transfer-based magnetic junction structures at frequencies ranging from 1 to 20 GHz and at full-width-half-maximum power linewidth at least 10,000 times below the center frequency. Phase-locking between magnetic-precession-induced microwave oscillation and additional input tune has also been demonstrated [65]. Future work in this area will likely be aimed at reducing the current density required for microwave generation, increasing device impedance, and, more significantly, increasing output signal amplitude and reducing the required external bias magnetic field.

Spin-transfer also affects the performance of magnetic read heads in modern hard drives [66–68], at times acting as a negative influence by amplifying the thermal and other magnetic noise of a read head, causing stability problems, decreasing the signal-to-noise ratio, and changing the dynamic characteristics of the read-head performance.

Spin-transfer-related magnetic excitation has also been observed to move magnetic domain walls in narrow ferromagnetic wires [69–74]. In fact, the interaction between spin-polarized current and a ferromagnetic domain wall was one of the first phenomena for which a spin-angular-momentum transfer process was considered [11, 12]. Recent experiments have demonstrated the unambiguous presence of a spin-torque term as the cause of domain wall motion under applied current. This mechanism [75–79], if harnessed at a low enough current density, could have significant implications for memory devices as well. A detailed discussion of the spin-transfer-related effects on magnetic domain wall motion is beyond the scope of this review.

In short, for applications in integrated circuits, the spin-transfer device must have a lower threshold current density—at least another order of magnitude less than what is demonstrated, and it must have much larger



Conceptual use of a three-magnetic-layer structure to increase the efficiency of a spin-current-induced magnetic switch. The vertical axis of the upper part indicates the amount of Fermi-level splitting $(\delta\mu)$ between the spin-up and spin-down electrons as a function of position x. The corresponding layer structure for the ferromagnetic films is illustrated in the lower part. See [80] for a detailed analysis that led to the associated prediction of a sixfold reduction in switching threshold current.

voltage output than the demonstrated values of several hundred μV . Various strategies are being proposed for achieving such improvements.

One proposal for reducing the current required to switch a nanomagnet was presented by Berger [80]. Figure 15 illustrates the proposal. For a free nanomagnet sandwiched between two oppositely fixed magnetic polarizer layers, Berger predicted a sizable enhancement of the spin-transfer effect, and an approximately sixfold net reduction of the threshold current. Several recent experiments [81] seem to confirm the existence of this enhancement, although a quantitative comparison with model results has yet to be made.

Several groups are also exploring the effect of spin-polarized tunnel current on a nanostructured magnetic "free" layer. Theoretical studies [82] point to the existence of a spin-torque-induced excitation similar to that found in a spin-valve type of nanojunction geometry. The main difference is the possibility of higher spin-polarization of the tunnel current. In addition, having significant nonlinear charge transport characteristics over a tunnel barrier changes the nature of spin-current transport, and the constraint on signal voltage amplitude discussed above for ballistic or diffusive spin-valves would, similarly, not limit the voltage output of a magnetic tunnel junction.

Early experimental reports from Grandis [83] and Cornell University [84] have confirmed the presence of a spin-transfer-induced magnetic reversal process in magnetic tunnel junction structures; see for example **Figure 16**. One challenge in these experiments is to

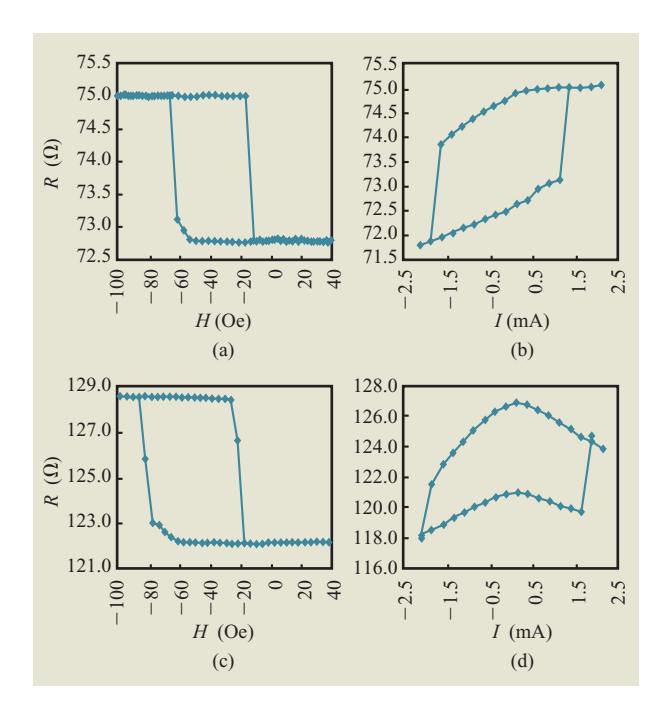


Figure 16

Two examples of a magnetic tunnel junction switching under a current bias. (a) and (c), magnetoresistance change when the junctions were swept by an applied magnetic field. (b) and (d), behavior of the corresponding junctions when swept by their bias current. The junctions were approximately 100 nm \times 200 nm in size, comprising a stack structure of ||Ta 2|NiFeCr 3.5|PtMn 14|CoFe 2|Ru 0.8|CoFe 2.2|AlO_x|CoFe 1|NiFe 2|Ta 5|| (numbers are layer thicknesses in nanometers). Adapted from [83], with permission; ©2004 American Physical Society.

quantitatively separate the spin-polarized tunneling current from other parallel channels of, e.g., pinhole conduction channels that may be present in such lowresistance tunnel devices.

Concluding remarks

In this overview, we have described how spin-transfer-induced magnetic excitation has been demonstrated in both all-metal spin-valve magnetic nanojunctions and magnetic tunnel junctions. The spin-transfer effect can generate persistent magnetic precession as well as complete reversal of the orientation of a nanomagnetic moment depending on bias current and field environment. The main effect of the spin-transfer is to reduce or increase the effective magnetic damping of the nanomagnet that is absorbing part of the spin-current, depending on the relative direction of the nanomagnetic moment with respect to the spin-polarization direction and the current flow direction of the spin-current. The spin-transfer-related effects become most visible when the

magnetic junction is small—around 100 nm or less in lateral dimensions and at a film thickness of less than 5 nm in the case of cobalt, for example.

Macro-spin dynamics capture the main experimental features well and constitute a good starting point for gaining a quantitative understanding of these new magneto-dynamics effects. For more quantitative and detailed understanding, finite-wavelength magnetic excitation must be carefully taken into account; in most cases this can only be done numerically.

Spin transfer has important implications for solid-state device applications. For magnetic random access memory (MRAM), it might potentially be used to locally writeaddress a nanomagnetic bit by passing an electrical (or spin) current through the particular nanomagnet. This write operation should not disturb the neighboring nanomagnetic bit, since it is easier to localize the writecurrent path than if the write operation were achieved through a current-induced magnetic field. It may also be possible to use a spin-transfer junction in its persistent precession mode, acting as an extremely compact tunable microwave generator. Spin transfer also affects the performance of the read heads in magnetic disk drives. In this case, the challenge is to avoid the amplification of thermal (and other) noises present in the read head by the spin-transfer excitation.

The current density required for spin-torque effect to result in magnetic reversal and persistent precession is still a bit too high for ready integration with CMOS technology. The threshold current density is for the moment limited primarily by the thin-film shapedetermined easy-plane anisotropy $4\pi M_s$. The reduction or elimination of this energy could reduce the threshold current, although the materials and processing challenge associated with such a proposal would be significant.

The signal voltage output from spin-valve-based spintransfer junctions is too low. These are all-metal-based junctions with very low impedances, rendering their integration with CMOS technology very challenging. Magnetic tunnel junctions, with their much wider range of impedances, should have much more potential as spintransfer switching (or oscillation) devices for circuit integration. This should become feasible once the spintransfer excitation current density is reduced to a level compatible with magnetic tunnel junctions having the desired impedance.

There are relatively stringent requirements on the switching current for reversing a nanomagnet if the nanomagnet is not to enter its super-paramagnetic state. The switching current required for retention of the nanomagnetic state at room temperature has been estimated to be of the order of 10 to 100 μ A, depending on its materials parameters.

Acknowledgments

I wish to thank D. W. Abraham, R. A. Buhrman,

W. Y. Chen, J. DeBrosse, W. J. Gallagher, J. A. Katine,

A. D. Kent, R. H. Koch, T. S. Kuan, D. J. Monsma,

B. Özylimaz, S. S. P. Parkin, D. C. Ralph, C. T. Rettner,

W. H. Rippard, M. J. Rooks, J. C. Slonczewski,

M. D. Stiles, B. D. Terris, M. Tsoi, P. L. Trouilloud,

and D. Worledge for stimulating discussions.

References

- G. Binasch, P. Grünberg, F. Saurenbach, and W. Zinn, *Phys. Rev. B* 39, 4828 (1989).
- M. N. Baibich, J. M. Broto, A. Fert, F. N. van Dau, F. Petroff, P. Etienne, G. Creuzet, A. Friederich, and J. Chazelas, *Phys. Rev. Lett.* 61, 2472 (1988).
- 3. S. S. P. Parkin, N. More, and K. P. Roche, *Phys. Rev. Lett.* **64**, 2304 (1990).
- 4. S. S. P. Parkin, IBM J. Res. & Dev. 42, 3 (1998).
- M. Tsoi, A. G. M. Jansen, J. Bass, W.-C. Chiang, M. Seck, V. Tsoi, and P. Wyder, *Phys. Rev. Lett.* 80, 4281 (1998).
- 6. J. Z. Sun, J. Magn. Magn. Mater. 202, 157 (1999).
- E. B. Myers, D. C. Ralph, J. A. Katine, R. N. Louie, and R. A. Buhrman, *Science* 285, 867 (1999).
- 8. J.-E. Wegrowe, D. Kelly, Y. Jaccard, P. Guittienne, and J.-P. Ansermet, *Europhys. Lett.* **45**, 626 (1999).
- J. A. Katine, F. J. Albert, R. A. Buhrman, E. B. Myers, and D. C. Ralph, *Phys. Rev. Lett.* 84, 3149 (2000).
- 10. J. Grollier, V. Cros, A. Hamzic, J. M. George, H. Jaffrès, and A. Fert, *Appl. Phys. Lett.* **78**, 3663 (2001).
- 11. L. Berger, J. Appl. Phys. 49, 2156 (1978).
- 12. L. Berger, J. Appl. Phys. 55, 1954 (1984).
- 13. L. Berger, J. Appl. Phys. 63, 1663 (1988).
- 14. C.-Y. Hung and L. Berger, J. Appl. Phys. 63, 4276 (1986).
- 15. L. Berger, J. Appl. Phys. 71, 2721 (1992).
- 16. L. Berger, Phys. Rev. B 54, 9353 (1996).
- Y. B. Bazaliy, B. A. Jones, and S.-C. Zhang, *Phys. Rev. B* 57, R3213 (1998).
- 18. J. C. Slonczewski, J. Magn. Magn. Mater. 159, L1 (1996).
- X. Waintal, E. B. Myers, P. W. Brouwer, and D. C. Ralph, *Phys. Rev. B* 62, 12317 (2000).
- 20. M. D. Stiles and A. Zangwill, Phys. Rev. B 66, 014407 (2002).
- E. M. Lifshitz and L. P. Pitaevskii, Statistical Physics, Part 2, Pergamon Press, Oxford, England, 1980, Ch. 7, Magnetism, p. 285
- Q. Yang, P. Holody, S.-F. Lee, L. L. Henry, R. Loloee,
 P. A. Schroeder, J. W. P. Pratt, and J. Bass, *Phys. Rev. Lett.* 72, 3274 (1994).
- F. J. Jedema, M. S. Nijboer, A. T. Filip, and B. J. van Wees, *Phys. Rev. B* 67, 085319 (2003).
- 24. J. C. Slonczewski, J. Magn. Magn. Mater. 195, L261 (1999).
- 25. M. D. Stiles and A. Zangwill, J. Appl. Phys. 91, 6812 (2002).
- M. D. Stiles, J. Xiao, and A. Zangwill, *Phys. Rev. B* 69, 054408 (2004).
- M. L. Polianski and P. W. Brouwer, *Phys. Rev. Lett.* 92, 026602 (2004).
- 28. J. Z. Sun, Phys. Rev. B 62, 570 (2000).
- J. Z. Sun, D. J. Monsma, T. S. Kuan, M. J. Rooks,
 D. W. Abraham, B. Oezyilmaz, A. D. Kent, and R. H. Koch,
 J. Appl. Phys. 93, 6859 (2003).
- J. Z. Sun, T. S. Kuan, J. A. Katine, and R. H. Koch, *Proc. SPIE* 5359, 445 (2004).
- 31. L. Berger, Phys. Rev. B 59, 11465 (1999).
- 32. M. Tsoi, A. G. M. Jansen, J. Bass, W.-C. Chiang, V. Tsoi, and P. Wyder, *Nature* **406**, 46 (2000).
- 33. J. Z. Sun, Phys. C 350, 3201 (2000).
- F. J. Albert, J. A. Katine, R. A. Buhrman, and D. C. Ralph, *Appl. Phys. Lett.* 77, 3809 (2000).

- J. Z. Sun, L. Chen, Y. Suzuki, S. S. P. Parkin, and R. H. Koch, J. Magn. Magn. Mater. 247, L237 (2002).
- M. A. McCord and M. J. Rooks, in Handbook of Microlithography, Micromachining and Microfabrication Vol. 1, Microlithography, P. Raichoudhury, Ed., SPIE Optical Engineering Press, Bellingham, WA, 1997, p. 202.
- J. Z. Sun, D. J. Monsma, M. J. Rooks, and R. H. Koch, *Appl. Phys. Lett.* 81, 2202 (2002).
- E. B. Myers, F. J. Albert, J. C. Sankey, E. Bonet, R. A. Buhrman, and D. C. Ralph, *Phys. Rev. Lett.* 89, 196801 (2002).
- S. Urazhdin, N. O. Birge, W. P. Pratt, Jr., and J. Bass, *Phys. Rev. Lett.* 91, 146803 (2003).
- S. I. Kiselev, J. C. Sankey, L. N. Krivorotov, N. C. Emley, R. J. Schoelkopf, R. A. Buhrman, and D. C. Ralph, *Nature* 425, 380 (2003).
- 41. Z. Li and S. Zhang, Phys. Rev. B 68, 024404 (2003).
- 42. Y. B. Bazaliy and B. A. Jones, Phys. Rev. B 69, 094421 (2004).
- J. Grollier, V. Cros, H. Jaffrés, A. Hamzic, J. M. George, G. Faini, J. B. Youssef, H. L. Gall, and A. Fert, *Phys. Rev. B* 67, 174402 (2003).
- S. I. Kiselev, J. C. Sankey, I. N. Krivorotov, N. C. Emley, M. Rinkoski, C. Perez, R. A. Buhrman, and D. C. Ralph, *Phys. Rev. Lett.* 93, 036601 (2004).
- 45. K.-J. Lee, A. Deac, O. Redon, J.-P. Noziéres, and B. Dieny, *Nature Mater.* 3, 877 (2004).
- R. H. Koch, J. A. Katine, and J. Z. Sun, *Phys. Rev. Lett.* 92, 088302 (2004).
- I. N. Krivorotov, N. C. Emley, J. C. Sankey, S. I. Kiselev,
 D. C. Ralph, and R. A. Buhrman, *Science* 307, 228 (2005).
- 48. Z. Li and S. Zhang, Phys. Rev. B 69, 134416 (2004).
- 49. D. M. Apalkov and P. B. Visscher; see http://arXiv:cond-mat/0405305-v1 (2004).
- 50. W. F. Brown, Phys. Rev. 130, 1677 (1963).
- G. Grinstein and R. H. Koch, *Phys. Rev. Lett.* **90**, 207201 (2003).
- D. M. Apalkov and P. B. Visscher, J. Magn. Magn. Mater. 286, 370 (2005).
- A. A. Tulapurkar, T. Devolder, K. Yagami, P. Crozat, C. Chappert, A. Fukushima, and Y. Suzuki, *Appl. Phys. Lett.* 85, 5358 (2005).
- S. Kaka, M. R. Pufall, W. H. Rippard, T. J. Silva, S. E. Russek, J. A. Katine, and M. Carey, *J. Magn. Magn. Mater.* 286, 375 (2005).
- J. Jorzick, S. O. Demokritov, B. Hillebrands, B. Bartenlian, C. Chappert, D. Decanini, F. Rousseaux, and E. Cambril, *Appl. Phys. Lett.* 75, 3589 (1999).
- W. H. Rippard, M. R. Pufall, S. Kaka, S. E. Russek, and T. J. Silva, *Phys. Rev. Lett.* 92, 027201 (2004).
- W. H. Rippard, M. R. Pufall, and T. J. Silva, *Appl. Phys. Lett.* 82, 1260 (2003).
- M. R. Pufall, W. H. Rippard, and T. J. Silva, *Appl. Phys. Lett.* 83, 323 (2003).
- Y. Ji, C. L. Chien, and M. D. Stiles, *Phys. Rev. Lett.* 90, 106601 (2003).
- B. Özyilmaz, A. D. Kent, D. Monsma, J. Z. Sun, M. J. Rooks, and R. H. Koch, *Phys. Rev. Lett.* 91, 067203 (2003).
- M. Tsoi, J. Z. Sun, M. J. Rooks, R. H. Koch, and S. S. P. Parkin, *Phys. Rev. B* 69, 100406R (2004).
- J. Z. Sun, B. Özyilmaz, W. Chen, M. Tsoi, and A. D. Kent, J. Appl. Phys. 97, 10C714 (2005).
- B. Heinrich, Y. Tserkovnyak, G. Woltersdorf, A. Brataas, R. Urban, and G. E. W. Bauer, *Phys. Rev. Lett.* 90, 187601 (2003).
- Y. Tserkovnyak, A. Brataas, and G. E. W. Bauer, *Phys. Rev. Lett.* 88, 117601 (2002).
- 65. M. R. Pufall, W. H. Rippard, S. Kaka, S. E. Russek, and T. J. Silva, "Modulation and Phase-Locking of Spin-Transfer-Induced Precessional Modes," Abstract HA-03, presented at the 49th Annual Conference on Magnetism and Magnetic Materials, IEEE and American Institute of Physics, 2004.

- M. Covington, A. Rebei, G. J. Parker, and M. A. Seigler, *Appl. Phys. Lett.* 84, 3103 (2004).
- M. Covington, M. AlHajDarwish, Y. Ding, A. Rebei, G. J. Parker, N. Gokemeijer, and M. A. Seigler, *J. Magn. Magn. Mater.* 287, 325 (2005).
- J.-G. Zhu, N. Kim, Y. Zhou, Y. Zheng, J. Chang, K. Ju,
 X. Zhu, and R. M. White, *IEEE Trans. Magn.* 40, 2323 (2004).
- A. Yamaguchi, T. Ono, S. Nasu, K. Miyake, K. Mibu, and T. Shinjo, *Phys. Rev. Lett.* 92, 077205 (2004).
- M. Kläui, C. A. F. Vaz, J. A. C. Bland, W. Wernsdorfer, G. Faini, E. Cambril, L. J. Heyderman, F. Nolting, and U. Rüdiger, *Phys. Rev. Lett.* 94, 106601 (2005).
- E. Saitoh, H. Miyajima, T. Yamaoka, and G. Tatara, *Nature* 42, 203 (2004).
- M. Yamanouchi, D. Chiba, F. Matsukura, and H. Ohno, Nature 428, 539 (2004).
- N. Vernier, D. A. Allwood, D. Atkinson, M. D. Cooke, and R. P. Cowburn, Europhys. Lett. 65, 526 (2004).
- J. Grollier, P. Boulenc, V. Cros, A. Hamzić, A. Vaurès,
 A. Fert, and G. Faini, Appl. Phys. Lett. 83, 509 (2003).
- 75. Z. Li and S. Zhang, *Phys. Rev. Lett.* **92**, 207203 (2004).
- 76. G. Tatara and H. Kohno, Phys. Rev. Lett. 92, 086601 (2004).
- 77. A. Thiaville, Y. Nakatani, J. Miltat, and Y. Suzuki, Europhys. Lett. 69, 990 (2005).
- 78. X. Waintal and M. Viret, Europhys. Lett. 65, 427 (2004).
- 79. S. Zhang and Z. Li, Phys. Rev. Lett. 93, 127204 (2004).
- 80. L. Berger, J. Appl. Phys. 93, 7693 (2003).
- 81. Y. Jiang, T. Nozaki, S. Abe, T. Ochiai, A. Hirohata, N. Tezuka, and K. Inomata, *Nature Mater.* 3, 361 (2004).
- J. Slonczewski, Phys. Rev. B 71, 024411 (2005); Phys. Rev. B 39, 6995 (1989).
- Y. Huai, F. Albert, P. Nguyen, M. Pakala, and T. Valet, *Appl. Phys. Lett.* 84, 3118 (2004).
- 84. G. D. Fuchs, N. C. Emley, I. N. Krivorotov, P. M. Braganca, E. M. Ryan, S. I. Kiselev, J. C. Sankey, D. C. Ralph, R. A. Buhrman, and J. A. Katine, *Appl. Phys. Lett.* 85, 1205 (2004).

Received March 17, 2005; accepted for publication June 3, 2005; Internet publication January 31, 2006

Jonathan Z. Sun IBM Research Division, Thomas J. Watson Research Center, P.O. Box 218, Yorktown Heights, New York 10598 (jonsun@us.ibm.com). Dr. Sun is a Research Staff Member in the Physical Sciences Department at the IBM Thomas J. Watson Research Center. He received a B.S. degree in physics from Fudan University, Shanghai, China, in 1984, and M.S. and Ph.D. degrees in applied physics from Stanford University in 1986 and 1989, respectively. For the following two years, he worked at Superconductor Technologies Inc. in Santa Barbara, California, as a member of the technical staff. He subsequently joined IBM at the Thomas J. Watson Research Center, where he has worked on superconducting and magnetic thin films and devices. Dr. Sun is a member of the American Physical Society and the Materials Research Society.

100